High-resolution P- and S-wave reflection studies of an intraplate structure
The Azambuja fault, Portugal

Ghose, Ranajit; Carvalho, João; Alves, Daniela V.; Santos, Luiz Alberto; Ressurreição, Ricardo; Alves, Paulo Henrique Bastos; Leote, Jaime

Important note
To cite this publication, please use the final published version (if applicable).
Please check the document version above.

High-resolution P- and S-wave reflection studies of an intraplate structure: The Azambuja fault, Portugal

Ranajit Ghose [a], João Carvalho [b,*], Daniela V. Alves [b,1], Luiz Alberto Santos [c,d], Ricardo Ressurreição [b], Paulo Henrique Bastos Alves [c], Jaime Leote [b,2]

[a] *Delft University of Technology, the Netherlands*
[b] *Laboratório Nacional de Energia e Geologia, Portugal*
[c] *Universidade Federal Fluminense, Brazil*
[d] *Petrobras, Brazil*

ABSTRACT

The Azambuja fault is a NNE trending structure located 50 km north of Lisbon, the capital and most populous city of Portugal. The fault has been considered as a possible source for the historical, large earthquakes. Understanding this fault is a priority in seismic hazard evaluation of this region. The fault has a clear morphological signature. Miocene and Pliocene sediments are tilted eastward and cut by steeply dipping mesoscale fault segments, presenting reverse and normal offsets with a net downthrow to the east. Neotectonic studies indicate a Quaternary slip on the fault of 0.05–0.06 mm/year. However, no direct evidence of the Azambuja fault affecting the Pleistocene or Holocene sediments was found so far. Here, we present the findings from high-resolution seismic reflection studies using both P- and S-waves over the Holocene deposits. The detection of small-throw faulting in ductile sediments is a challenging task. We show that multiple signatures, like perturbations in the reflection hyperbolae visible in shot and CMP gathers, interruptions of reflectors in stacked sections, lateral seismic velocity variations obtained by horizon velocity analysis, all at coincident locations, strongly suggest that the activity of the Azambuja fault has affected the Holocene sediments in the study area. The lateral velocity variations are corroborated by wavepath eikonal traveltime tomography and velocity analysis supported by seismic modeling. By means of 2D viscoelastic modeling, we explain the absence of fault-related diffractions and negligible back-scattered energy from the fault. Using data from nearby boreholes, we find that the 15 ka old alluvium cover has indeed been disturbed by the presence of shallow fault strands. Considering the estimated vertical throws and the empirical relationships between fault length, co-seismic rupture and magnitude, a slip rate of 0.07 mm/y, slightly larger than previously thought, is expected for this fault.

1. Introduction

The Lower Tagus Valley, located in the central mainland of Portugal, includes the densely populated (>3.5 million) area of Lisbon. The region has been affected in the past by multiple earthquakes causing loss of lives and considerable material damages. It is, therefore, important to correctly evaluate the seismic hazard of the region. In the last 800 years, large plate-boundary earthquakes occurred in 1755 and 1969, whereas local intraplate moderate-sized earthquakes occurred in this area at least in 1344, 1531 and 1909 (Fig. 1). In this research, we study the Azambuja

fault, an intraplate structure located about 50 km north of Lisbon (Fig. 1). This fault presents one of the best evidence of neotectonic activity in this area (Cabral et al., 2004).

The Azambuja fault is a NNE oriented structure located in the Lower Tagus Cenozoic Basin. In the Azambuja village area, the published geological maps (Zbyszewski and Veiga Ferreira, 1967; LNEG, 2010) show a fault contact between the Miocene and the Pliocene sediments along an extension of about 7 km. These sediments are located to the SE of the fault trace, in a lower altimetric position. At the surface, the fault manifests as a distributed deformation zone where Miocene and

---

Pliocene sediments are tilted eastward and cut by steeply dipping mesoscale sub-faults presenting reverse and normal offsets with a net downthrow to the east, as observed in a few outcrops near Azambuja (Cabral et al., 2004).

The fault has a clear morphological signature, represented by a 15 km long east-facing scarp with a maximum height of 80 m near Azambuja, where the fault presents a higher vertical offset (Cabral et al., 2004). From the Tagus river alluvial plain at Azambuja to the Pontével Creek in the NNE, the scarp is about 7 km long (Fig. 2a, see also Carvalho et al., 2014). It is interrupted by a 3 km wide gap at the Pontével Creek, continuing further NNE for about 5 km. According to Cabral et al. (2004), the creek coincides with a 1 km left-lateral stepover, where the fault may be segmented at the crustal level. The authors also suggest that the Pontével Creek location is controlled by a pronounced active synform, as suggested by the opposite tilting of the Miocene sediments on both margins. To the NNE, the Azambuja fault probably extends until the NW-SE oriented Vale de Santarém fault zone (D'Amato et al., 2009, see Fig. 2b), which is part of a WNW-NW trending fault system that affects the Lower Tagus Valley region (Carvalho et al., 2014; Carvalho et al., 2017). The two deformation zones seem to control the disposition of the Pliocene sediments on the downthrown block of the Azambuja fault. Based on oil-industry (P-wave) seismic profiles, Cabral et al. (2004) assumed the prolongation of the fault to the SSW, on the Tagus alluvial plain, at least up to the S1 profile. The orientation of the primary P-wave profile S1 was roughly E-W, and it was located approximately at the same latitude as Benavente (Fig. 2a). P-wave reflection data also allowed to characterize the fault as a high-angle thrust fault that caused a vertical offset of about 200 m on the base of the Cenozoic sediments located below the Holocene alluvial cover. Considering this prolongation, we estimate an extension of approximately 20 km for the southern segment.

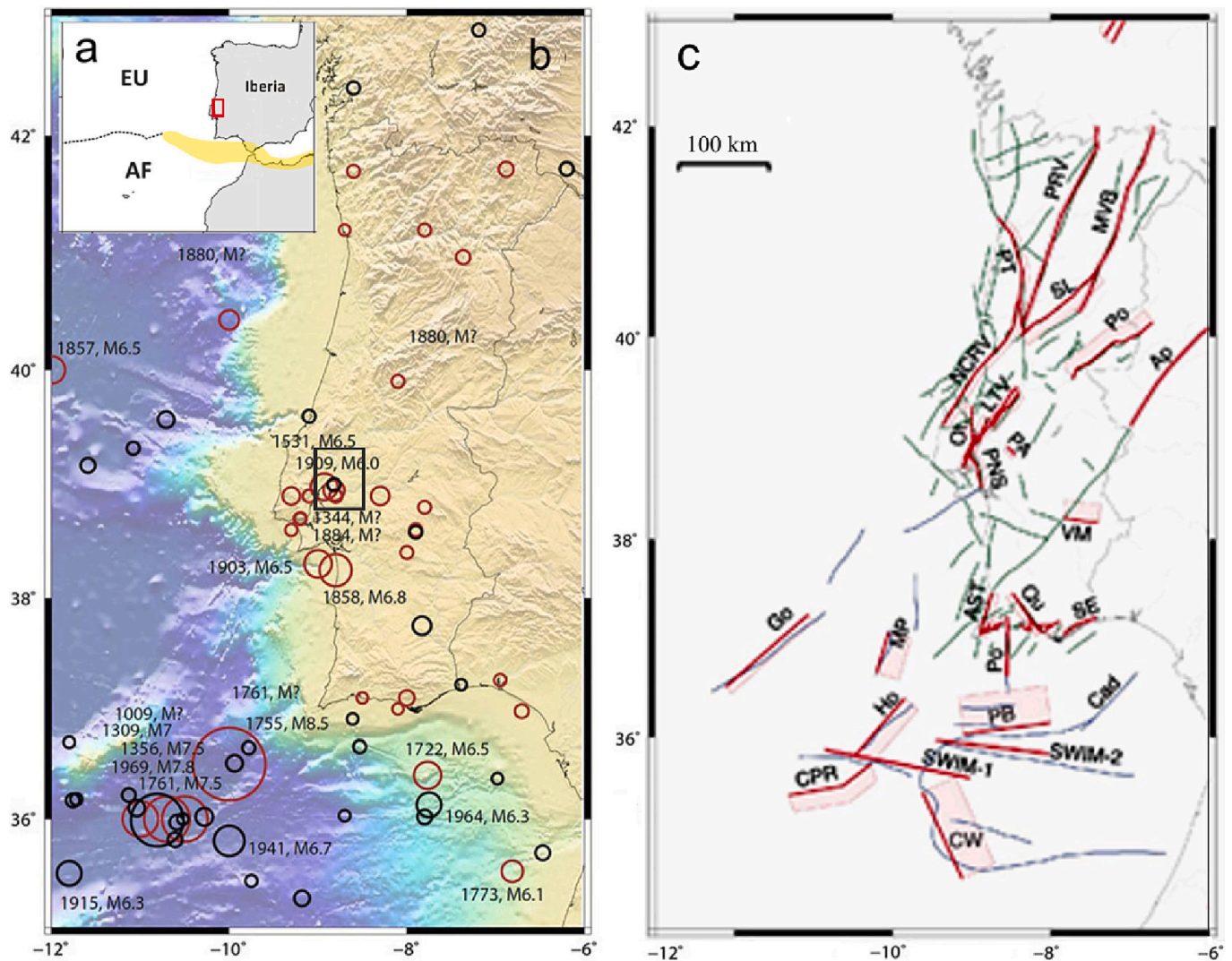The Azambuja fault is considered to be an active fault (Cabral et al.,

Fig. 1. (a) Seismotectonic setting of the mainland Portugal and the adjacent area (adapted from Custódio et al., 2015), illustrating also the location of the study region (red rectangle) in relation to Eurasian (EU) and African (AF) plates. The yellow shade marks a zone of diffused deformation. (b) Historical (till 1910) and instrumental earthquakes (source: Portuguese Institute for the Sea and Atmosphere [IPMA]) with M ≥ 5 displayed as circles, where the radius correlates with the earthquake magnitude. For M ≥ 6 earthquakes, the dates and the respective magnitudes are given. "M?" means unknown magnitude. The black rectangle shows the location of the present study area. (c) Potentially active regional faults. PT: Porto-Tomar fault; PRV: Penacova-Régua-Verín fault; MVB: Manteigas-Vilariça-Bragança fault; SL: Seia-Lousã fault; Po: Ponsul fault; NCRV: Nazaré-Caldas da Rainha-Vimeiro fault; Ot: Ota fault; LTV: Lower Tagus Valley fault; PNS: Pinhal Novo-Setúbal fault; PA: Porto Alto fault; AP: Alentejo-Placencia (Messejana) fault; VM: Vidigueira-Moura fault; SE: S. Estevão fault; Qu: Quarteira fault; Po: Portimão fault; AST: Azambuja-S. Teotónio fault; Go: Gorringe fault; MP: Marquês do Pombal fault; Ho: Horseshoe fault; CPR: Coral Patch Ridge fault; PB: Portimão Bank fault; CW: Cadiz Wedge; SWIM-1/2: SouthWest Iberia Margin lineaments; Cad: Cadiz fault. (For colour representation in this figure, the reader is referred to the web version of this article.)
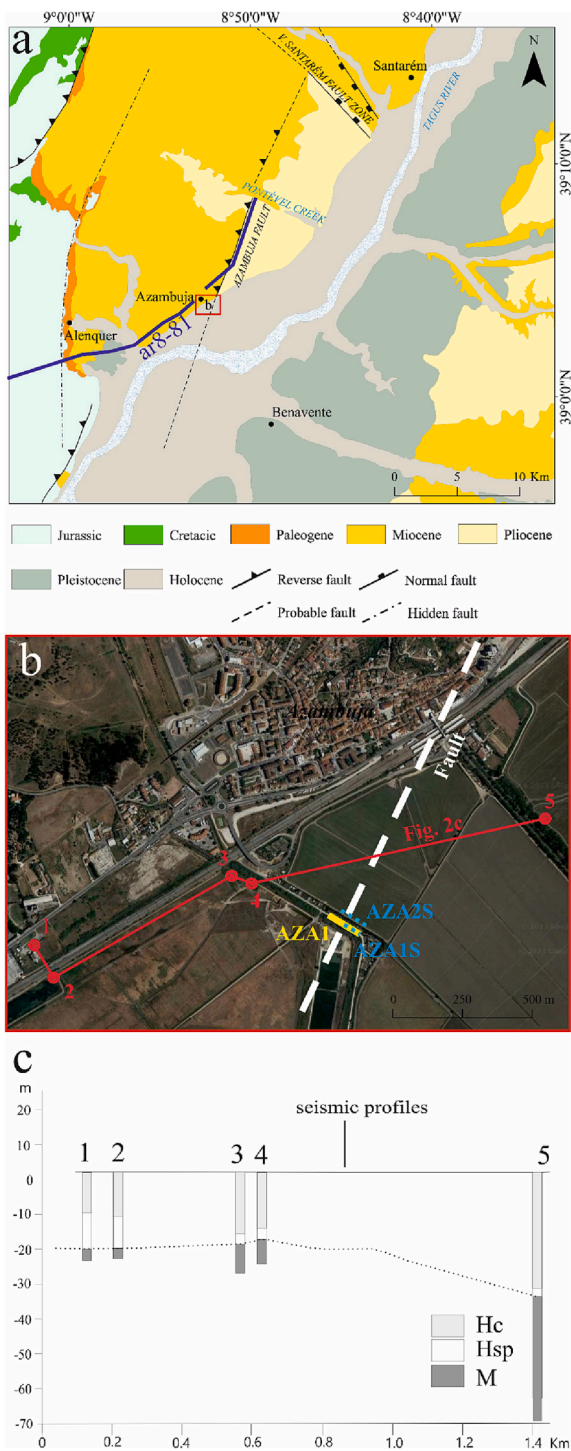
Fig. 2. (a) Location of the seismic reflection studies relative to the Azambuja fault scarp. The blue line represents oil-industry P-wave seismic profile (ar8-81), shown in Fig. 3; the red rectangle indicates the area of the shallow seismic reflection profiling performed in the present research. The geology is adapted after LNEG (2010); (b) Google Earth™ image showing the location of the P-wave (continuous yellow line and marked AZA1) and S-wave (dashed blue lines, marked as AZA1S and AZA2S) shallow reflection profiling performed in this study, the possible southwards extension of the Azambuja fault (white dashed line) and the nearby boreholes (numbered red circles) used in interpretation; (c) cross-section derived from these borehole data, illustrating the lateral correlation of the base of the Holocene. Hc - Holocene clay, silt and sand layers; Hsp - Holocene sand and pebble layers; M - Miocene units. (For colour representation in this figure, the reader is referred to the web version of this article.)

2003, 2004). Cabral et al. (2013) hypothesized that this fault could be the seismogenic source for the 1909 Benavente earthquake. For the characterization of its seismogenical potential, Cabral et al. (2004) assumed two length values: 15 km, considering a southern sector in which the fault segmentation near Pontével behaves as a barrier for seismic rupture; and 25 km, assuming a whole-length rupture. Based on this and on the vertical displacement of several Quaternary erosional surfaces, they estimated a moment magnitude of 6.4–6.7 for maximum earthquakes, with a recurrence period of 10,000–25,000 years. The Quaternary slip of the fault was estimated to be in the range 0.05–0.06 mm/year. However, the activity of this fault in the Holocene was not established so far.

Due to small slip-rates and a long recurrence time-interval in the area (Cabral et al., 2004; Carvalho et al., 2006; Vilanova et al., 2014), the surface ruptures are easily erased by erosion and/or are covered by the river Tagus sedimentation. Dating of the alluvium cover in the nearby area has established an age of 15 ka for the 50 m thick column of sediments (Carvalho et al., 2006). These sediments are composed of sands and clays with a layer of pebbly sands at the base. The Holocene sediments cover a Miocene sedimentary succession of clayey sandstones, sandstones, clays, and fossiliferous marls and limestones (Zbyszewski and Veiga Ferreira, 1968). In the alluvial plain south of Azambuja the Pliocene formation is absent. The Pliocene sediments must have been eroded by the Quaternary incision of the Tagus river.

The flat alluvial plain and the lack of outcrops also prevent the detection of the fault trace in the Holocene sediments. For these reasons, in order to study the fault activity in the Tagus alluvial plain, a careful use of selected, high-resolution geophysical methods is needed. The seismic reflection method is one of the most suitable exploration methods in clayey and shallow-water-table environments, and has been applied many times in the past to locate seismogenic faults (e.g., Shtivelman et al., 1998; Floyd et al., 2001; Williams et al., 2001; Kaiser et al., 2011; Ghose et al., 2013). In this type of environment, ground penetrating radar often fails to produce useful results, and electrical and electromagnetic methods, besides having generally a lower resolution than seismic in a clayey environment, require a powerful electrical source due to the presence of salty water and shallow water table.

In the present research, we have at first tested the shallow P-wave seismic reflection method to investigate the possible presence of the Azambuja fault below the Holocene sediments at the Tagus alluvial plain, south of the known fault outcrops. The location of this profile is shown in Fig. 2b. We have found indications of multiple shallow fault strands in the P-wave reflection data, but the resolution was not sufficient. Subsequently we have carried out high-resolution S-wave reflection surveys at the same site (see location in Fig. 2b), and have identified a number of different signatures in the data that might indicate the presence of deformation in the shallow soil layers due to synsedimentary faulting (e.g., Sugiyama et al., 2003; Inazaki, 2004; Harris, 2009; Carvalho et al., 2016, Onyebueke et al., 2018; Hunter et al., 2022). We have checked the plausibility of these features in the S-wave reflection dataset through forward modeling, mimicking the field condition and the acquisition set up. To corroborate the results, we have also performed continuous horizon velocity analysis (HOVA), velocity analysis supported by seismic modeling (VASSM), and first-arrival traveltime tomography (FATT) using wavepath eikonal traveltime (WET) inversion.

In the following sections, we present at first the different methodologies and the details of field data acquisition and data processing. We then present the results and their interpretation. Based on our findings, the characteristics of the Azambuja fault in terms of fault throw, fault length, slip rate, and their seismogenic implications are discussed.

2. Methodology

2.1. Fault trace identification in the alluvial plane: P-wave seismic reflection

Fig. 2a shows the location of the nearest outcrop of the Azambuja fault relative to the site of the present seismic reflection studies. Detailed locations of the P-wave profile and 5 nearest boreholes are marked in Fig. 2b. The profile locations were selected assuming a straight prolongation of the fault to the SSW from the outcrop. Prior to this study, the only seismic profile to image the fault outcrop was acquired in 1981 by CGG for the oil industry. In this P-wave profile, which is shown in Fig. 3, the fault is imaged as a steep, deep-rooted structure, but the acquisition parameters of this seismic profile did not allow a proper imaging of the shallow subsurface. Other regional faults such as the Ota fault (Wilson et al., 1989; Carvalho et al., 2017) or the Lower Tagus Valley Fault zone (see Canora et al., 2021 and the references therein) are visible in the profile. The near-surface is poorly imaged in the oil-industry profile due to the acquisition geometry. Such a low-resolution image does not allow verifying if the fault affects the near-surface where mostly the Neogene sediments outcrop. Therefore, it was decided to try to locate the fault on the SSW of the known fault outcrop, in the alluvial plain covered by the Holocene sediments (Fig. 2a).

After initial walkway noise tests, shallow P-wave reflection data were acquired in this study using 48 active receiver channels, and 1.5 m interval for both sources and receivers. During processing, in order to homogenize the acquisition geometry along the entire profile length and prevent appearance of acquisition footprints, we reduced the data to an end-on geometry using 36 active channels. This resulted in a constant CMP fold of 18 along the entire profile, and a source-to-the-nearest-receiver distance of 4 m. An accelerated weight drop (250 kg) seismic source was used to generate the P waves; the total trace length was 1 s, with a time-sampling interval of 0.25 ms.

The data were acquired over a flat, hard, asphalt road; the receivers were planted close to the edge of the road. The water table at the time of data acquisition was approximately at 2 m. The compacted surface condition was responsible for a frequent second hit of the source-plate on the ground after the main hammer blow, which caused a second arrival at a time of around 300 ms. These reverberations were difficult to eliminate from the shot gathers through data processing. For this reason, the noise-cone muting had to be performed. Data processing included geometry installation, bandpass filtering, first-arrival muting, f-x deconvolution, residual (surface consistent) static correction, velocity analysis, and CMP stacking.

The data were migrated after stacking. This was followed by filtering and amplitude enhancement. Unmigrated and migrated stacked sections for the Azambuja P-wave reflection profile are shown in Fig. 4a and b. Using an 1D velocity function obtained from the stacking velocity field, we have depth-converted the time section. The tentative depth section is shown in Fig. 4c.

2.2. Imaging shallow fault strands under Holocene sediments: S-wave seismic reflection

The indications of faulting in the shallow sediments noticed in the P-wave reflection data needed greater details of the fault strands, appropriate for the purpose of fault-throw quantification and deformation assessment. For this reason, two shallow, S-wave seismic reflection profiles were planned. In such unconsolidated soils, S-waves can provide much superior resolution than P waves primarily because of the very low S-wave velocity in soft soils, but also due to the good sensitivity of S-wave to subtle changes in soil composition and texture (Ghose and Goudswaard, 2004; Harris, 2010; Ghose et al., 2013). Considering the typical values for P- and S-wave velocities in shallow soil layers in this region, and the frequency of the observed P- and S-waves in our seismic experiments, the vertical resolution in seismic trace data (assuming Rayleigh criterion of one-quarter of the wavelength) is about 2–3 m for P-waves and 0.3–0.5 m for S-waves (Carvalho et al., 2006, 2016; Ghose et al., 2013).

S-wave reflection surveys were carried out at two closely located sites with very different surface conditions. As the area was highly cultivated, it was possible to carry out seismic investigations only at these two sites. The first S-wave profile was 55 m long, and it overlapped the first part of the shallow P-wave reflection profile (Fig. 2b). The second S-wave profile, parallel to the first profile, was 90 m long, and was located at 30 m distance from the first profile, along a pathway made of compacted alluvium (Fig. 2b). The seismic source used for S-wave generation was a wooden plank hit on its sides with a metal hammer. The wooden plank was pressed with the wheels of a heavy car, providing a good coupling with the ground. As in the previous case, 48 geophones were used in data acquisition, however during data processing the number was reduced to 36 geophones per shot in order to homogenize the acquisition geometry and the CMP fold along the entire profile and prevent imaging artefacts. The shortest source-receiver offset was 4 m. The receiver spacing was 0.75 m; it was carefully chosen such that there was no spatial aliasing in the data. The seismic wavefield was recorded for 1 s, with 0.25 ms data sampling interval.

As both sites were flat, no elevation static correction was necessary. Also, little P-wave contamination was observed in the S-wave data, and

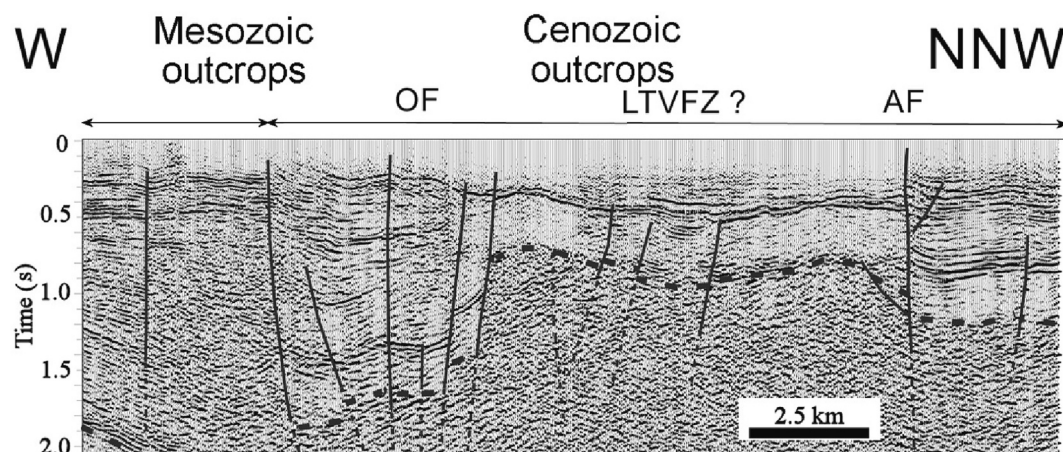**Fig. 3.** P-wave seismic reflection profile acquired for oil-industry by CGG, showing the Azambuja Fault (AF) as a steep-dipping structure. See similar interpretation in Cabral et al. (2004) of the Azambuja fault along this same profile. Black continuous line - top of the Mesozoic; thick dashed line - top of the Palaeozoic; OF - Ota fault; LTVFZ - Lower Tagus Valley Fault Zone. See Fig. 2 for the profile location.
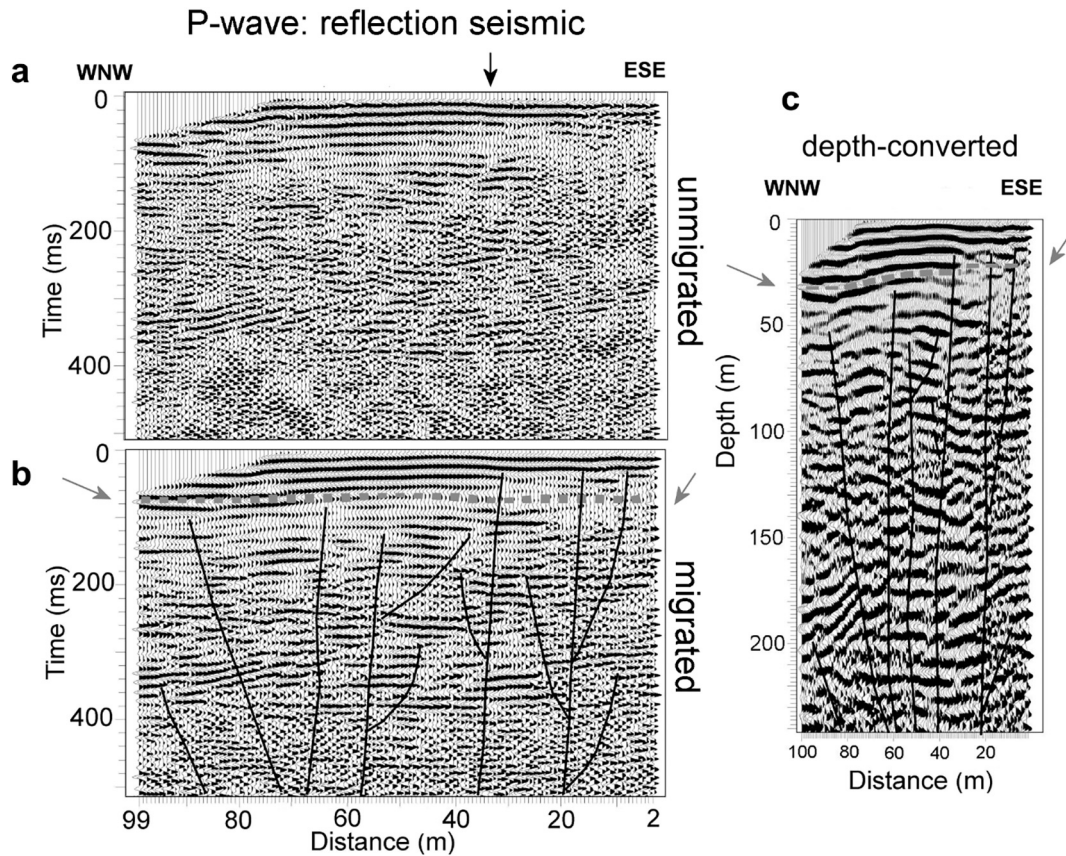
P-wave: reflection seismic

Fig. 4. (a) Unmigrated, (b) post-stack time-migrated, and (c) depth-converted stacked sections for the shallow P-wave seismic reflection profile at Azambuja. Arrow at the top margin indicates location of an important change found in the alluvial sediments. Vertical throws in the Holocene are not resolved in P-wave data (vertical resolution 2–3 m), but the eastern part of the section suggests deformation of alluvial sediments. In the depth-converted section, the horizontal dashed line (in grey) marks the interpreted base of the Holocene alluvium layers based on data from nearby boreholes, while the black vertical lines represent interpreted fault strands.

therefore left- and right-hitting of the source-plank and subsequent subtraction of datasets were not necessary. Only one side of the source-plank was hit. This reduced the possibility of loss of resolution, which happens when the source wavelets from left and right hits are not sufficiently similar. Surface (Love) waves were absent in the first profile due to the hard asphalt road laid above the low-velocity alluvium. At the second site too, the compaction of the top-soil due to the passage of vehicles was responsible for the generation of little Love waves by the sledge-hammer source.

The data processing sequence consisted of geometry installation, bandpass filtering, first-arrival muting, spectral whitening (25–70 Hz), velocity analysis, and CMP stacking using an 1D velocity function. Surface consistent statics were not applied to avoid possible cycle skipping and prevent disturbing any subtle signature of faulting in the soft sediments. As with the P-wave, data were afterwards DMO-corrected and then post-stack migrated using a phase-shift algorithm (Gazdag and Squazzero, 1984). This was followed by filtering and amplitude enhancement. Unmigrated and migrated stacked sections for the Azambuja S-wave reflection profiles are shown in Figs. 5 and 6. As before, using an 1D velocity field derived from the stacking velocities for each profile, tentative depth sections were obtained from the stacked time sections (Fig. 7).

2.3. Evidence from the velocity field: HOVA, VASSM and FATT

To check the tectonic origin of these discontinuities/disturbances in CMP, shot gathers and in the stacked sections, we examined the velocity field at each CMP location (CMPs are spaced at 0.38 m) using automatic horizon velocity analysis (HOVA), following the approach proposed by

Ghose et al. (2013). For this purpose, the most prominent seismic horizons were chosen in a stacked section, and a time window around the automatically picked peak amplitude at these horizons was fixed. The semblance value for the chosen reflection event in each CMP gather was then estimated for various stacking velocities. The result is shown in Figs. 9a and b for several reflection horizons in profile 1 and 2, between 100 and 600 ms two-way-time.

Next, we performed velocity analysis supported by seismic modeling (VASSM), which can be described as follows. Velocity analysis performed on CMP gathers from profile AZA1S provided the stacking velocity for the S-wave reflections. From this stacking velocity, we calculated the interval velocity in time (Dix, 1955). This velocity function was converted to depth to generate the initial model, Vs_0. Common-receiver-stacking was then performed to produce a brute-stack. Although the acquisition design of AZA1S uses an end-on configuration, the common-receiver brute-stack resembles that of the end-on geometry (Fig. 9c1) and has the same characteristics of a plane-wave survey, as if all the sources were turned on at the same (zero) time.

The thus-obtained brute-stack constituted a compacted version of the dataset. Let us call this d_{obs}. Aided by acoustic forward modeling, we then generated a plane-wave synthetic seismic dataset d_{calc}. The objective of the forward modeling was to fit the kinematics of d_{obs} with that of d_{calc}. To perform acoustic wavefield modeling, we needed velocity and density fields. For the velocity, we used Vs_0 (S-wave interval velocity). As we did not have the density field, we estimated it from the time-migrated section using the following procedure. First, the time-migrated section was depth-converted using Vs_0. The resulting depth section was normalized, multiplied by a scale factor, and a constant value of 2.0 Kg/m^3 was added. Though the obtained density values are
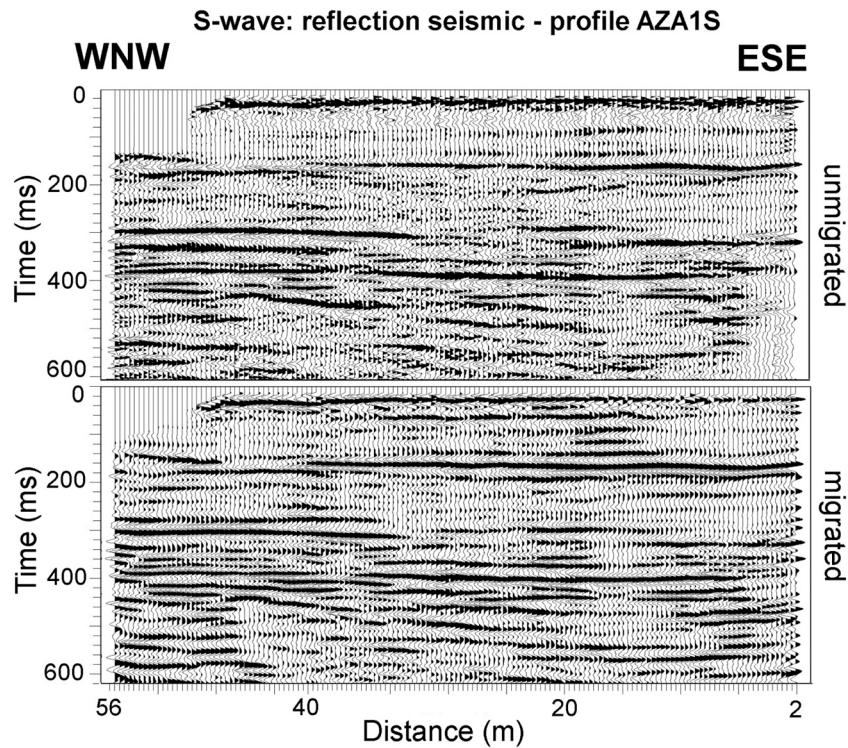
Fig. 5. Unmigrated (top) and post-stack time-migrated (bottom) stacked sections for the shallow S-wave reflection profile 1 (AZA1S), which is partially coincident with the shallow P-wave reflection profile (Fig. 4).
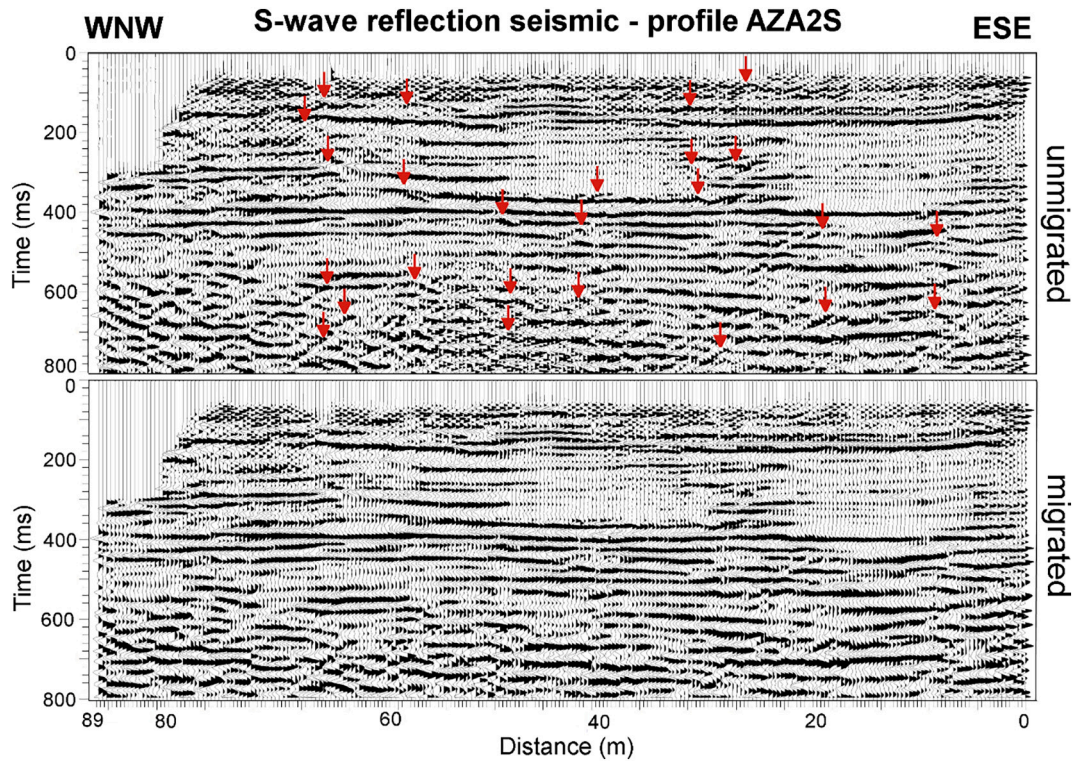
Fig. 6. Unmigrated (top) and post-stack time-migrated (bottom) stacked sections of the shallow S-wave reflection profile 2 (AZA2S), acquired 30 m north of and parallel to the shallow P-wave profile and the S-wave profile 1 (Figs. 4 and 5, respectively). Arrows in the unmigrated stack indicate possible diffractions whose locations match with the location of the interpreted fault strands shown in Figs. 7 to 10. Several other diffractions - not marked – can also be traced; they probably originate at deeper fault strands which are not investigated in this research.

S-wave: Depth section - profile AZA2S

S-wave: Depth section - profile AZA1S

Fig. 7. Depth-converted S-wave reflection profiles 1 and 2 using an average 1D velocity function obtained from the stacking vel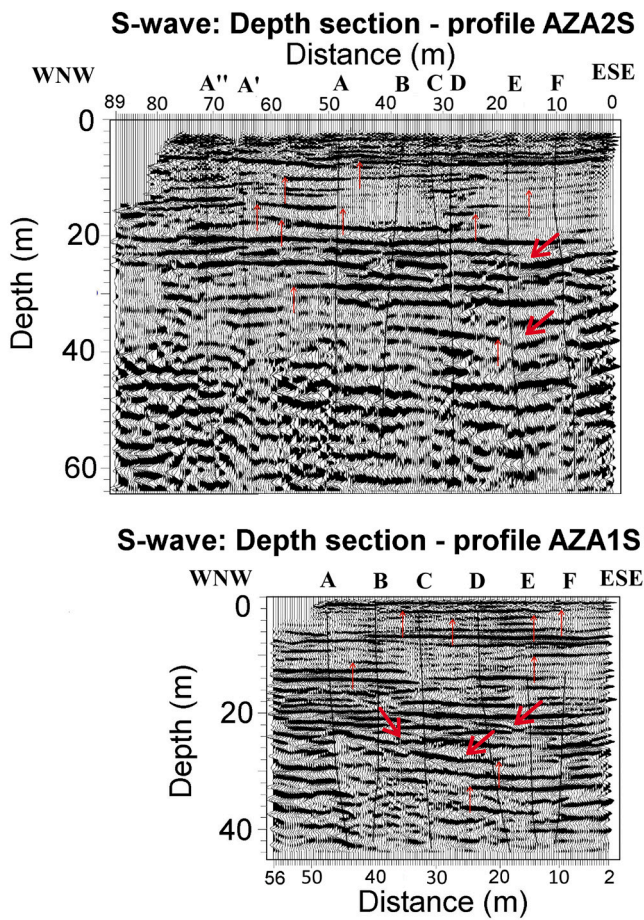ocity. The letters on the top and the black vertical lines indicate locations of interpreted major fault strands at places where anomalies are marked in Figs. 8 to 10. Downward-pointing thick arrows indicate possible fluvial channels. Some of the upward-pointing, thin arrows, located laterally away from the interpreted fault-strand locations, might mark other geological discontinuities (lithological, grain size, fluid content, etc.). Thickness of the alluvial cover is estimated at 20 m, based on the seismic pattern observed in stacked sections and borehole data (see Fig. 2).

typical of sediments of the same age and lithological composition found in Portugal (e.g., Carvalho et al., 2011), the value does not need to be accurate. This is because the resulting density section (ρ_0) has only the purpose of adding contrasts to the model; its absolute value does not matter, as the main objective of the modeling is to fit the kinematics of the calculated data to that of the observed data.

The model zero, m_0 (Vs_0, ρ_0), used for the first simulation delivers a synthetic dataset d_{calc0} that does not completely honor the main mapped horizons. Using the misfit between events at d_{calc0} and d_{obs}, we manually updated the S-velocity model to Vs_1. With Vs_1, another version of the density field was calculated using the same procedure as described above. The next round of modeling is then performed delivering the synthetic data d_{calc1} (Fig. 9c2) that fits the main events of the field stacked data d_{obs} (Fig. 9c1). The obtained result lends credibility to the Vs_1 field (Fig. 9c3) as being representative of the subsurface below profile AZA1S.

As in HOVA, VASSM velocity field shows horizontal changes that are spatially correlated with the location of the interpreted fault strands. To further corroborate these results, we picked first breaks in all shot gathers in S-wave data and performed first-arrival traveltime tomography (FATT) using wavepath eikonal traveltime (WET) inversion (Schuster and Quintus-Bosz, 1993; Watanabe et al., 1999). An 1D

velocity model with a vertical gradient was used as the initial model. The result of tomography is shown in Fig. 9d for the profile AZA2S.

2.4. Viscoelastic forward modeling of observed S-wave reflections

In order to investigate the presence/absence of back-scattered energy in the shot and CMP gathers, and check other evidences of shallow faulting detected in the S wavefield, we performed 2D viscoelastic modeling for profile 1 (where no diffractions were observed) using a finite difference code (Thorbecke and Draganov, 2011) and a crossline S-wave source. The frequency band (35–120 Hz) of synthetic data was similar to that in field data. Noise was not added to synthetic shot gathers. The velocity model was based on borehole data and the 1D velocity field derived from the stacking velocities. We emplaced narrow low-velocity zones at locations of the fault strands (Fig. 10a) as interpreted in this study with a velocity which is 10 m/s lower than that of the surrounding sediments, as found in the results of HOVA, VASSM and FATT.

We did not incorporate complex fault-zone features that are often observed in open trenches (e.g., Bonilla and Lienkaemper, 1990; Rockwell et al., 2009; Figueiredo et al., 2011; Suter et al., 2011; Canora et al., 2021), such as fault branching, dipping or curved faults, anisotropy, etc. The effect of the surficial, highly compacted layer, likely to be causing negligible Love waves in the field data in profile 1, was partially reproduced in our modeling through introducing an 1 m thick surface layer with high velocity. This high-velocity top layer indeed caused a reduction of amplitude of the Love wave train.

Fig. 10b shows a synthetic shot gather (source located at 24 m) corresponding to the layered model shown in Fig. 10a - which mimics profile 1 but without the presence of any fault. The field shot gather with the source at the same position (at 24 m) is shown in Fig. 10c. Fig. 10d illustrates the same synthetic shot gather but for a model with several faults (Fig. 10a), and no attenuation (Q = ∝). Very similar reflection events (marked as r1–r4) and reflection moveouts are visible between field and synthetic data. However, the amplitude of the first reflection (r1) is much weaker in the synthetic gather due to the strong amplitude of the Love wave train (sw in Fig. 10b). The Loves waves are negligible in the field shot gather. However, strikingly, the undulations and discontinuities in the S-wave reflection moveout that we observe in the field shot gathers are marked, and they are very similar between synthetic and field shot gathers. These locations also match well with the location of the disturbances noticed in the stacked sections and the lateral velocity changes observed in HOVA panels and in the results of VASSM and FATT (Figs. 5, 6, 7 and 9).

3. Results

3.1. P-wave data

In the migrated and depth-converted shallow P-wave image (Fig. 4b and c) we overlaid the interpreted fault strands and the base of the Holocene alluvial cover. For this interpretation we have used data from several boreholes located within 1 km distance, and geological information (Zbyszewski and Torre de Assunção, 1965; Zbyszewski and Veiga Ferreira, 1968). These boreholes, with simplified geological logs, are shown in Fig. 2c; they were drilled earlier for water supply and geotechnical investigation purposes. The borehole data provided a good control on the depth of the Holocene alluvium in this area.

According to borehole data, the sandy and clayey alluvium is thicker to the east of the profile (borehole 5 in Fig. 2c), reaching a depth of about 33 m. To the west of the seismic reflection profile (boreholes 1–4, Fig. 2c), an average depth of 17 m is found for the base of the alluvium. At this depth, a several-meters-thick pebble layer marks the transition to Miocene sediments. The assemblage of the shallowest seismic reflectors shows strong amplitude and a good lateral continuity (up to 80 ms two-way-time, or approximately 38 m depth), and is in reasonable

agreement with the depth of the alluvium sediments as observed in boreholes.

The discontinuous nature of the reflection events in this section suggests the possible presence of dipping fault strands with some splay faults reaching close to the surface, in agreement with the geological outcrop data (Cabral et al., 2004). We suspect discontinuities at several locations along this seismic profile (Fig. 4b, c). The location at approximately 38 m seems to mark a sudden change in the thickness or the properties of the alluvium cover, suggesting the possible presence of a major fault plane (Fig. 4b). This and other fault strands located in the eastern part of the seismic section are approaching the surface. The unmigrated image indicates that the impressions of faults are less affected by the seismic data-processing steps. These fault strands possibly disturb nearly the entire alluvium cover at this site (see following section).

3.2. S-wave stacked sections

The stacked sections of both profiles (AZA1S and AZA2S) show several discontinuities and amplitude changes along the reflectors that are consistent across depth at lateral locations around 10, 15–20, 38–41 and 48 m in profile 1, and at around 10, 20, 30, 39, 50, 60 and 65–70 m in profile 2 (Fig. 7). These discontinuities might represent locations of fault strands (black lines in Fig. 7) that correspond to an extension of the NNE-oriented Azambuja fault zone, which outcrops 1 km further north of this site (see Fig. 3). Otherwise, these discontinuities could also be caused by lateral lithological variations. However, lateral lithological changes occur at a scale of several meters to tens of meters, and they do not occur concentrated in time/depth at a fixed locality, as observed in the seismic sections in Figs. 5 to 7. These lateral changes are also present in the profile, and a few are indicated in Fig. 7. A tentative base of the alluvium cover, based on borehole data (Fig. 3) and on the seismic pattern observed in the stacked sections, is set to a depth of 20 m. Most

of the interpreted fault strands (except at location 15 m in profile 1 and locations 19 and 60 m in profile 2) approach the surface - at least till horizon 1 (~150 ms two-way-time or about 7 m in depth).

To ensure the validity of such interpretation, it is useful to search for multiple signatures of faulting in the seismic data at these locations (Ghose et al., 2013; Carvalho et al., 2016). All shot and CMP gathers were inspected in search of disturbances or discontinuities in the reflection hyperbolae. Fig. 8 shows the representative field shot gathers from profiles 1 and 2. For profile 1, the shot gathers have only been bandpass-filtered because of the good data quality and the presence of negligible noise and surface waves. For profile 2, the shot gathers have been muted to remove the first arrivals and the surface waves, in order to increase the visibility of the reflection events. A careful look at the shot gathers in Fig. 8 reveals the presence of undulations and discontinuities in the reflection moveout and a sudden change in reflection amplitudes around the locations of the interpreted fault strands. These perturbations are visible in S-wave shot gathers and CMP gathers, and are similar to those found in other sites where faulting is known to be present and seismic modeling was performed earlier (Ghose et al., 2013; Carvalho et al., 2016). The lateral positions of these disturbances are close between the stacked sections and the shot gathers in both profiles. The deformation that occurs in soft sediments is commonly ductile in nature. This will be discussed further in a later section.

3.3. HOVA, VASSM and FATT of S-wave data

The WET tomogram for the AZA2S profile shows, in the first 2 m below the surface, horizontal velocity variations similar to and spatially correlated with those obtained from HOVA and VASSM. Major lateral velocity changes are found at approximately 20 m and 40 m lateral distances (Fig. 9). These variations extend from the surface till the investigation depth (about 15 m), and are in agreement with the locations of the interpreted fault strands in the stacked sections. Considering
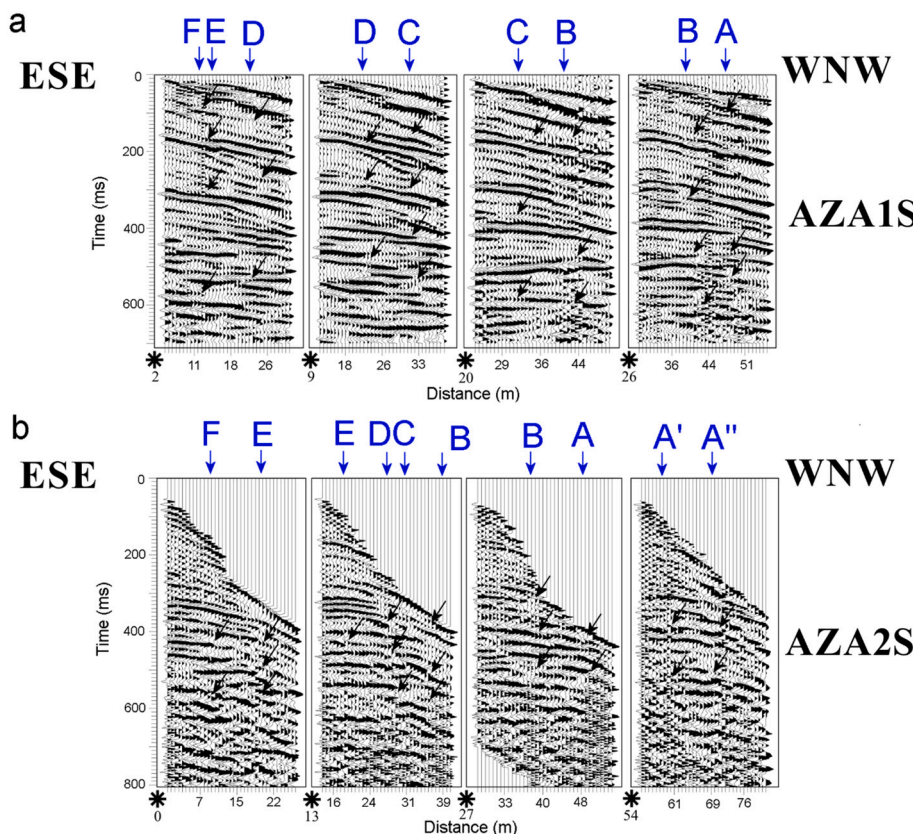

Fig. 8. (a) Raw field shot gathers from S-wave reflection profile 1 (AZA1S), with 10–100 Hz bandpass filtering. Undulations, amplitude changes, and breaks are apparent in reflection hyperbolae at locations which match with the locations of abrupt changes in velocity found in HOVA analysis (Fig. 9) and perturbations in the reflection events in the stacked sections (indicated by arrows). The letters in the top margin indicate the same locations as marked in stacked sections and HOVA panels shown in Figs. 5 to 7 and 9. (b) Same as (a) but for profile 2 (AZA2S); here the field shot gathers have been top-muted to remove direct wave and surface waves, to increase the visibility of the reflection events. The black stars with a number below indicate shot locations in meter.
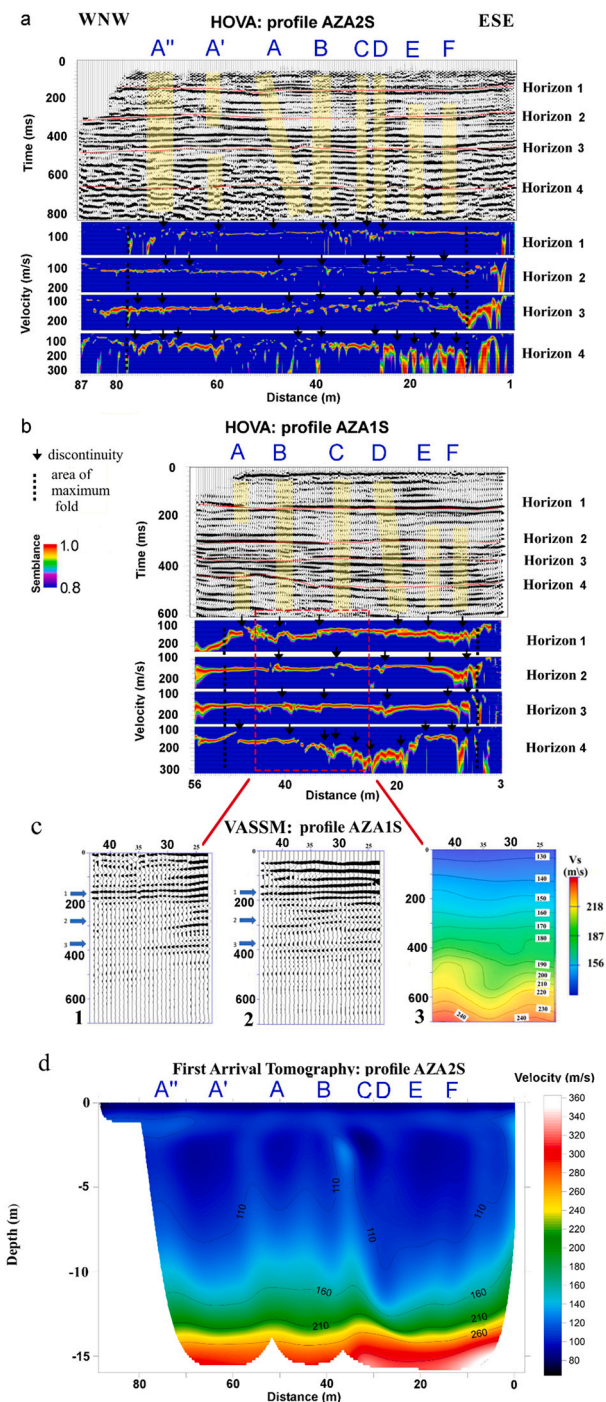
Fig. 9. (a) Results of HOVA for chosen seismic horizons (indicated by numbers) in S-wave profile 2 (AZA2S); (b) results of HOVA for selected horizons in S-wave profile 1 (AZA1S). Letters at the top margin indicate locations of sharp velocity changes that coincide with the locations of interruptions and changes in the amplitude/phase of the reflection events observed in stacked sections and shot gathers (Figs. 5 to 8). Yellow shaded zones show position of the interpreted fault strands; (c) VASSM in the central part of profile AZA1S: c1) brute stack of a part of the profile AZA1S, where the arrows mark the same events 1, 2 and 3 shown in c2; c2) synthetic brute stack of AZA1S profile; c3) S-wave velocity model (Vs₁) used to calculate the synthetic brute stack shown in c2; (d) FATT for profile AZA2S. A, B, C, D are plotted in the same horizontal scale and position as in (a). (For colour representation in this figure, the reader is referred to the web version of this article.)

the observed changes in the nature/continuity of the reflectors in the stacked sections, the detected velocity changes also occur nearly at the same lateral positions and over similar two-way-time or depth ranges. These matching observations support strongly the possibility of localized presence of shallow fault strands as opposed to lateral lithological changes. At the AZA1S profile site, the first arrivals are weak, probably due to the presence of the compacted top layer. As a result, first arrivals could not be picked with confidence, and hence the tomogram is not calculated.

Fault zones/strands have typically a lower seismic velocity relative to the adjacent sediments (e.g., Mooney and Ginzburg, 1986; Hough et al., 1994; Mamada et al., 2002; Nielsen et al., 2008; Yang et al., 2011). We observe that in both AZA1S ad AZA2S datasets, there are clear velocity changes in the main reflection horizons at the locations of the interpreted fault strands (Fig. 9). The magnitude of these velocity changes increases with depth and sediment age. At many of these locations, step-like velocity changes can be observed, which are indicative of synsedimentary faulting in soft sediments (Vanneste et al., 1999; Neuwerth et al., 2006; Ghose et al., 2013; Carvalho et al., 2016). These faults, which develop during or soon after deposition of sediments, are aided by over-pressured, under-compacted conditions typically present in buried muds (Elliot and Ladio, 1981). Such conditions are likely to have been present during the sedimentation of the Holocene soil layers in the Lower Tagus Valley, made of water saturated sands, clays and silts.

Simultaneous observation of discontinuities in the main reflectors in S-wave stacked sections, disturbances and amplitude changes in shot and CMP gathers, lateral velocity changes along the prominent reflectors, all approximately at the same lateral and vertical locations, point to the presence of shallow fault strands in the seismic lines. The lateral positions of the observed disturbances can be slightly deviated from the linear geometry assumed in Figs. 7 to 9, as fault strands are often curved or branched in a complex manner. Other disturbances caused by lateral geological changes (lithological, grain size, fluid content, etc. changes) add to the perturbations caused by fault strands. According to nearby borehole data (Fig. 3), the depths at which most of these fault strands are observed correspond to Holocene sediments.

Such sharp changes at the location of a fault strand should, however, produce also diffractions and/or back-scattered energy from the fault plane or the fault-damaged zone (e.g. Kawahara and Yamashita, 1992; Chávez-Pérez et al., 1998; Nielsen et al., 1998; Ghose et al., 2013), even in soft soils where the deformation is plastic and the velocity changes relative to the adjacent sediments can be small (Ghose et al., 2013; Carvalho et al., 2016). Seismic diffractions are caused by localized structures and discontinuities. For the S-wave profile 1 (Figs. 5 and 8a), we did not trace such diffracted events at the interpreted fault locations. However, for S-wave profile 2, it was possible to identify indication of diffractions and back-scattered energy mostly in the unmigrated stacks (Figs. 6 and 8b).

3.4. Viscoelastic modeling of S-wave data

The apparent mismatch between field and synthetic shot gathers regarding the presence of backscattered energy (*bs* in Fig. 10e and f) was difficult to explain in the first instance. We found such backscattered energy in synthetic shot gathers (Figs. 10d to f) but not in field data (Figs. 5, 6, 7, 8 and 10c). To investigate this, we performed viscoelastic forward modeling. When we introduced attenuation ($Q_S = 60$) in our model, we noticed that the backscattered reflections became significantly weak, compared to the model with no attenuation (Fig. 10d).

This value of the quality factor for S wave ($Q_S = 60$) is higher (i.e., lower attenuation) than that generally found in soft sediments at shallow depths and at the frequency range of our data. Kudo and Shima (1970) found Q_S ranging 5–20 in unconsolidated sediments, while Jeng et al. (1999) measured Q_S values between 4 and 34 in one of their studied sites using a frequency dependent Q_S estimate. For the first 6 m
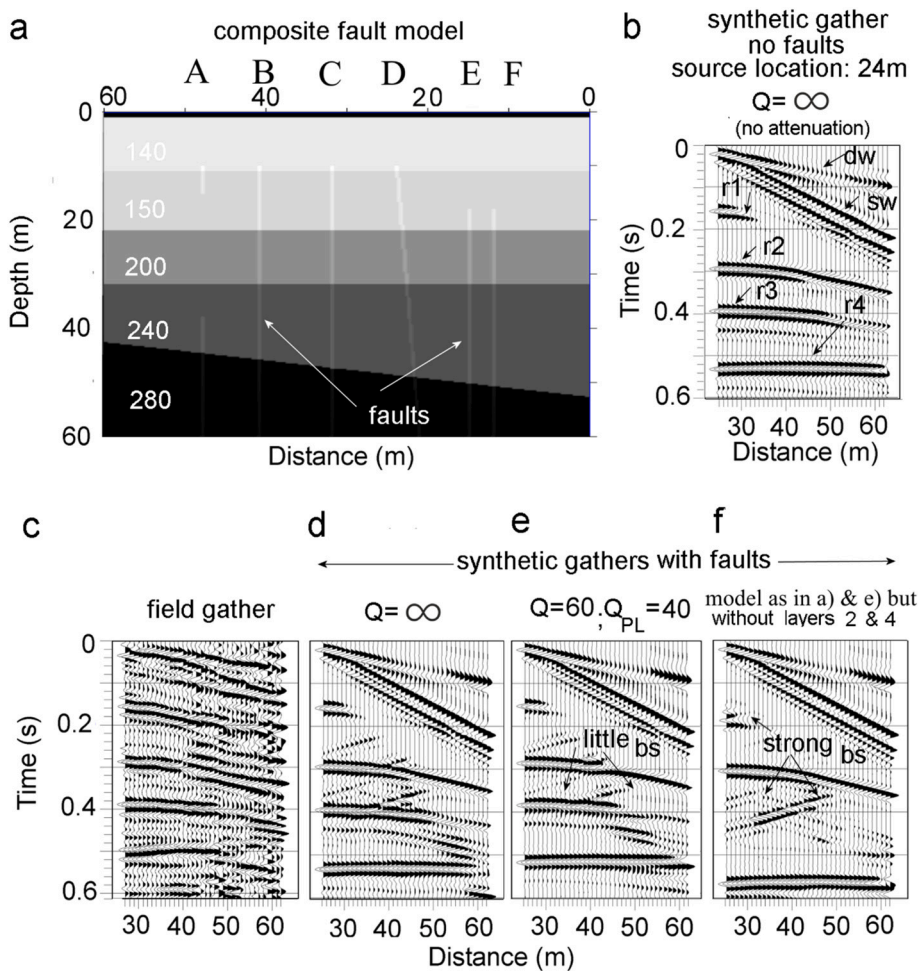
Fig. 10. (a) Velocity model for profile AZA1S used to generate the synthetic shot gathers presented in Fig. 10b, d-f. Possible fault strands are modelled as narrow low-velocity zones with relative vertical displacement and an assumed velocity contrast of 10 m/s with the adjacent sediments. Numbers (in white) indicate shear-wave velocities in the model obtained from HOVA analysis. Layer depths are based on observation in nearby boreholes. (b) A synthetic shot gather representing profile 1, obtained using the velocity model in a) but without any faults, for a source located at 24 m. dw - direct wave; sw - surface waves; r_i - reflection at the top of layer i + 1. Q_S - quality factor for S waves. (c) The field shot gather at the same source location as in b). Synthetic shot gather for the model shown in a) with no attenuation ($Q_S = \infty$). (d) Same shot gather but for a model with attenuation $Q_S = 60$. Q_{PL} is quality factor of the pebble layer. bs- back-scattered reflections from the fault strands. (e) Same synthetic shot gather for an overall attenuation of $Q_S = 60$ and only for layer 1 (top layer) $Q_S = 40$. (f) Same shot gather as in (e) but without layers 2 and 4. Notice the increase in the back-scattered energy.

of soil, Jongmans (1990) reported Q_S of 1.2 to 2.8. Wang and Li (2018) reported a Q_S value varying between 16 and 100 in the first 1 km of a sedimentary sequence. The Q_S values in the range of 40 to 60 as used in our modeling are higher than many earlier reported values, but such lower attenuation might be caused by the shallow water table at this site and the stress accumulation in the fault zone.

Crane (2013) and others have indeed reported that seismic attenuation varied not only with frequency but also with water saturation and stress. Quality factor was found to increase with stress and water saturation, though a local minimum for the quality factor was observed at partial saturation, and a higher value corresponded to total saturation. The sandy nature of some sediment layers in the study area, the proximity of the Tagus river potentially causing total water saturation in many layers, and the stress built up in the close vicinity of the Azambuja fault - all together may have contributed to the higher value for Q_S that we find through forward modeling explaining our observation. The present-day stress-field, as obtained from borehole breakouts (Ribeiro et al., 1996) and from earthquake mechanisms (Borges et al., 2001; de Vicente et al., 2018), is NNW to NW oriented. This stress orientation is in agreement with the orientation of the strain field derived from plate velocity measurements using data from the Global Navigation Satellite Systems (GNSS) stations (e.g., Neves et al., 2014), and has presumably led to the stress accumulation at the NNE-SSW oriented structures, such as the Azambuja fault.

As mentioned above, the back-scattered energy is nearly absent in stacked sections and shot gathers, especially in the profile AZA1S. In this context, we notice in the borehole data from Azambuja site the consistent presence of a pebble layer at the base of the alluvium. S-wave

reflections from the top of this layer constitute the first primary reflection event that we observe in the AZA1S shot gathers at about 160 ms two-way-time (r1 in Fig. 10). This pebble layer is not present at this depth at several other earlier-investigated sites in the Tagus river delta, e.g., Vila Franca de Xira or Castanheira do Ribatejo sites (Carvalho et al., 2016; 2020). The attenuation of seismic waves is expected to be high (i. e., low Q_S values) in such pebble layers and also in the first (top) layer where the sediments are less compacted and more disturbed by human activities. In our modeling, if we assign a higher attenuation than before ($Q_S = 40$ instead of 60) to this pebble and surface layers, and unchanged attenuation in other layers, then we notice slightly less back-scattered energy in the synthetic shot gather (Fig. 10e). The highly attenuating top layer and the layer with pebbles at the bottom might indeed have contributed to the occurrence of little or no back-scattering in the data of profile AZA1S. In Fig. 10f we show the same model with faults as in Figs. 10d to e, the same attenuation properties as in Fig. 10e but without layers 2 and 4. The presence of back-scattered energy is now enhanced. Apparently, the lack of back-scattered energy in the field data of AZA1S profile might have an additional contribution from the presence of multiple reflection horizons. Similarly, the existence of multiple thin layers of sand, clay and silt, and the softness of the Holocene alluvial sediments might be responsible for the relatively few diffractions that we observe in the AZA2S field data.

3.5. Discussion: Implication on seismic potential of the Azambuja fault

In the two S-wave stacked sections AZAS1 and AZAS2 (Figs. 5 to 7), a number of shallow fault strands seem to approach the surface, reaching

as shallow as 3.5 ± 0.5 m (see Figs. 7 and 9d). Since the alluvium sedimentation rate in this region is highly variable (Ramos et al., 2002), the age of the deformed, most-surficial sediments cannot be estimated. We have shown that the above-mentioned possible fault strands correspond to velocity changes at lateral locations where discontinuities and perturbations are noticeable in the reflection hyperbolae in shot gathers (Fig. 8), as well as diffractions in the stacked section of AZA2S (Fig. 6). Viscoelastic forward modeling shows that those observed perturbations in shot gathers can be explained by the presence of slightly lower-velocity, sub-vertical fault strands within the sediment layers (Fig. 10). Impression of such localized, low-velocity zones appears in the results of FATT and VASSM (Fig. 9). All these signatures are very different from the signs of lateral lithological changes in the soil. Lateral lithological changes such as channel structures, sediment truncations and interfingering associated with fluvial regimes, and grain-size changes can be visible in high-resolution seismic data, including the data in this research. However, lithological changes are generally not as vertically continuous as we observe in our data. The apparent continuity of some of the reflectors across the interpreted fault strands is probably due to the small fault-throw relative to vertical resolvability of our seismic data (which is ~0.4 m) and the size of the Fresnel zone.

The data shows the existence of a broad deformation area with multiple fault-dislocation planes similar to the diffused deformation zone identified in the outcrop by Cabral et al. (2004). The existence of this deformation zone at a location which lies on the extension of the surface-mapped Azambuja fault suggests, together with borehole data, a strong likelihood that the deformation correspond to the Holocene activity of the fault. We do not have borehole data on our seismic lines to directly decipher the vertical offset of a particular geological/seismic horizon. From P- and S-wave stacked sections it is difficult to infer the vertical throw for the interpreted fault strands with accuracy. A minimum vertical offset of about 1 m can be inferred from the stacked sections.

The stacked sections presented in this article (Figs. 5 to 7) suggests sharp disruptions of a few seismic horizons, which can only be caused by large fault movements. This change of seismic character and of reflector continuity from one site to the other, as found in our study, might indicate strike-slip motion on the fault (e.g. Bally, 2002; Tün et al., 2010; Gold et al., 2013), although the Azambuja fault was characterized by Cabral et al. (2004) as a thrust fault, with no mention of strike-slip movement. Ignoring the strike-slip component of faulting in our analysis might have caused under-estimation of slip rate and coseismic displacement to some extent. Taking into account a vertical offset (above an assumed minimum) of 1 m in the last 15 ka, we obtain a 0,066 mm/y slip rate - which is in the same order as the one estimated by Cabral et al. (2004) based on displaced Pleistocene geomorphic features.

In this work we consider a total length of about 30 km for the Azambuja fault, assuming that its northern sector extends until the NW-SE Vale de Santarém fault zone, as both structures seem to control the deposition of Pliocene sediments in this region. This means that the fault trace might extend 2–3 km further to the NNE than the fault scarp. Its total prolongation in the SSW direction in the Tagus alluvial plain is not known, although compatible deformation was identified on the S1 profile located 11 km SSW of the Azambuja village (Cabral et al., 2004). As for the maximum and minimum possible rupture lengths of the Azambuja fault, we propose about 30 km to be the entire length, while 18 km if we consider the rupture along the segment that extends from the Pontével Creek to the Tagus alluvial plain, where the vertical offset is greater.

We use the above values for the fault length (L) and a co-seismic vertical throw (D) of 1 m in the following empirical relationships (Stirling et al., 2002):

$$Mw = a + b \, Log \, (L), \tag{1}$$

$$Log \, (D) = a + b \, Log \, (L), \tag{2}$$

Table 1
Moment magnitude (Mw) for the of maximum expected earthquake and the average surface displacement (D) estimated using the regression equations of Stirling et al. (2002). *a* and *b* are the regression parameters, L the fault length. We used i) a minimum fault length of 18 km considering the Azambuja Fault segmentation by the Pontével Creek, and ii) a 30 km long fault in case of no segmentation.

Formula	L (km)	a	b	Mw or D (*, m)
(1)	18	5.88	0.80	6.9
(2)	18	0.06	0.18	1.93(*)
(1)	30	5.88	0.80	7.1
(2)	30	0.06	0.18	2.12(*)

where Mw is the moment magnitude of an earthquake, *a* and *b* are the regression parameters. We obtain the results that are summarized in Table 1.

The Azambuja fault can produce $M_W > 6$ earthquakes with a surface displacement of about 2 m, even if we consider the segmentation of the fault at the Pontével. Secondly, we are only considering here the vertical displacement and ignoring the strike-slip component, as implied by the seismic reflection data. The significance of the strike-slip component is, however, not known. Therefore, the values presented in Table 1 are underestimates.

Important information like recurrence and slip rates, coseismic displacement, time of the most recent (unrecorded) large earthquake, etc. might be obtained in the future from trenching. However, the opening of a trench and obtaining reliable ground-truthing data in an area where the water table is very shallow (about 1 m) might prove difficult. Trenching may also provide inconclusive results, as the nearby trench data (at Vila Franca de Xira, see Fig. 3) indeed show that the top 3–4 m of the near-surface is composed of homogeneous dark clays, where the fault strands are locked (Carvalho et al., 2020).

Another option could be drilling boreholes across the expected fault strands. This may not only confirm the presence or absence of fault strands, but also may provide insights into the fault activities over time. The methodology presented here can be a powerful tool to unravel the earthquake/fault activities and to provide useful information prior to opening a trench or drilling. When trenching or drilling boreholes is not a viable option, shallow, high-resolution seismic studies as reported here might be crucial and the only means to reach the goal and improve the quality of seismic hazard assessments.

4. Conclusions

The Azambuja fault is known to have deformed the Miocene-to-Pliocene sediments. Post-Pliocene (Pleistocene) deformation has earlier been speculated, but so far it was not possible to directly establish its effect on the Holocene sediments. In this article, we have presented the first evidence that this fault might have affected the alluvial sediments deposited over a time period of about 15 ka. The last time the fault ruptured at this site is earlier than this time, given the shallow location of the deformed sediments. However, considering the irregular sedimentation rates well-known for this area, the time of the most recent rupture cannot be estimated with certainty.

We acquired P- and S-wave shallow seismic reflection datasets over the Holocene alluvial sediments at about 1 km SW of the Azambuja fault outcrop - which is visible in the Neogene terrains. Shallow P-wave reflection data and borehole data indicated that a steeply dipping fault affected the Neogene sediments and possibly also the alluvial cover at the location of our experiments. However, P-wave data lacked sufficient resolution.

Analyses of high-resolution S-wave reflection data could detect multiple signatures of soft sediment deformations and shallow faulting. Such faulting has probably affected the shallow alluvium layers at the location of our seismic experiments. The evidences are visible on S-wave

stacked sections, in velocity fields extracted automatically using horizon velocity analysis (HOVA), first-arrival traveltime (FATT) tomograms, and velocity analysis supported by seismic modeling (VASSM), on CMP and shot gathers, and supported by synthetic shot gathers obtained from viscoelastic forward modeling with realistic geometry. We have found at the same locations interruptions in the reflection horizons in stacked sections, undulations, and discontinuities in the reflection moveout in shot and CMP gathers, and sharp lateral velocity changes in the results of HOVA. These detected changes have been further corroborated by the results of wavepath eikonal traveltime (WET) inversion and VASSM. The results of viscoelastic forward modeling incorporating shallow steeply dipping fault strands emplaced in the Holocene layers further supported the interpretation. The modelled synthetic shot gathers are remarkably similar to field shot gathers. The little presence of back-scattered and diffracted energy in the field shot gathers might be due to the presence of an attenuating surface layer of pebbles at this site. This pebble layer is observed in the nearby boreholes. Our modeling, however, suggests that the absence of back-scattered energy is primarily due to the presence of several alternating layers of sands and clays that produce multiple reflections, which camouflage the relatively small-amplitude back-scattered reflections.

Some of the fault strands are found to approach the very near-surface region - to as shallow as 3–4 m depth. A minimum vertical throw of 1 m is estimated (on S-wave stacked section and shot gathers) for the alluvium layer, related to the last seismogenic surface rupture that occurred in this area. The estimated minimum and maximum fault lengths vary between 18 km and 30 km. Using empirical relationships, we obtain a maximum expected M_W of 7.1, with a coseismic surface displacement of approximately 2 m for a rupture length of 30 km, and an expected maximum magnitude of 6.9 with a coseismic displacement of 1.93 m. The slip rate was estimated to be ~0.07 mm/y for the last 15 ka. These obtained values will be very useful to improve the assessment of seismic hazard potential in the region of Lower Tagus Valley and the metropolitan Lisbon. Trenching is difficult to carry out in the study area. The methodology presented here, together with borehole data, can be a powerful tool to help identifying the recent deformation affecting the alluvium cover in this region and deducing seismic hazard-assessment parameters.

Credit author statement

Ranajit Ghose: Conceptualization, Methodology, Validation, Investigation, Supervision, Formal analysis, Writing - Review & Editing.
João Carvalho: Conceptualization, Methodology, Software, Validation, Investigation, Writing - original draft.
Daniela V. Alves: Methodoloy, Software, Data curation, Formal analysis, Visualization.
Luiz Alberto Santos: Methodology, Software, Formal analysis, Writing - original draft. Visualization.
Henrique Bastos Alves: Software, Formal analysis. Visualization.
R. Ressurreição: Investigation, Writing - original draft. Visualization.
Jaime Leote: Data curation.

Declaration of Competing Interest

The authors declare that they have no known competing financial interests or personal relationships that could have appeared to influence the work reported in this paper.

Data availability

Data will be made available on request.

Acknowledgements

References

Bally, A.W., 2002. Atlas of seismic stratigraphy. In: Bally, A.W. (Ed.), AAPG Studies in Geology, v. 27, vol. 1. American Association Petroleum Geologists.
Bonilla, M.G., Lienkaemper, J.J., 1990. Visibility of fault strands in exploratory trenches and timing of rupture events. Geology 18 (2), 153–156.
Borges, J.F., Fitas, A.J., Bezzeghoud, M., Teves-Costa, P., 2001. Seismotectonics of Portugal and its adjacent Atlantic area. Tectonophysics 337, 373–387.
Cabral, J., Moniz, C., Ribeiro, P., Terrinha, P., Matias, L., 2003. Analysis of seismic reflection data as a tool for the seismotectonic assessment of a low activity intraplate basin- the lower Tagus Valley (Portugal). J. Seismol. 7, 431–447.
Cabral, J., Ribeiro, P., Figueiredo, P., Pimentel, N., Martins, A., 2004. The Azambuja fault: an active structure located in an intraplate basin with significant seismicity (lower Tagus Valley, Portugal). J. Seismol. 8, 347–362.
Cabral, J., Moniz, C., Batló, J., Figueiredo, P., Carvalho, J., Matias, L., Teves-Costa, P., Dias, R., Simão, N., 2013. The 1909 Benavente (Portugal) earthquake: search for the source. Nat. Hazards 69, 1211–1227. https://doi.org/10.1007/s11069-011-0062-8.
Canora, C., Vilanova, S.P., De Pro-Diáz, Y., Pina, P., Heleno, S., 2021. Evidence of surface rupture associated with historical earthquakes in the Lower Tagus Valley, Portugal. Implications for Seismic Hazard in the Greater Lisbon Area. Front. Earth Sci. 9 https://doi.org/10.3389/feart.2021.620778.
Carvalho, J., Cabral, J., Gonçalves, R., Torres, L., Mendes-Victor, L., 2006. Geophysical methods applied to fault characterization and earthquake potential assessment in the lower Tagus Valley, Portugal. Tectonophysics 418, 277–297.
Carvalho, J., Rabeh, T., Bielik, M., Szlaiova, E., Torres, L., Silva, M., Carrilho, F., Matias, L., Miranda, J.M., 2011. Geophysical study of the Ota- V.F. Xira-Lisboa-Sesimbra fault zone and of the Lower Tagus Cenozoic basin. J. Geophys. Eng. 8, 395–411.
Carvalho, J., Rabeh, T., Dias, Rui, Dias, Ruben, Pinto, C.C., Oliveira, T., Cunha, T, Borges, J., 2014. Tectonic and Neotectonic Implications of a New Basement Map of the Lower Tagus Valley, Portugal. Tectonophysics 617, 88–100. http://dx.doi.org/10.1016/j.tecto.2014.01.017.
Carvalho, J., Ghose, R., Alves, D., Leote, J., 2016. Earthquake faulting-related deformation in soil evidenced in S-wave shallow reflection data: field results from Portugal. Geophysics 81 (5), IM97–IM108. https://doi.org/10.1190/geo2015-0040.1.
Carvalho, J., Pinto, C., Rabeh, T., Dias, R., Torres, L., Borges, J., Torres, R., Duarte, H., 2017. Tectonic Evolution of an Intraplate Basin: The Lower Tagus Cenozoic Basin, Portugal. Basin Res. 29 (5), 557–636. https://doi.org/10.1111/bre.12193.
Carvalho, J., Alves, D., Cabral, J., Ghose, R., Borges, J., Dias, R., Ramalho, E., Caldeira, B., Casacão, J., Leote, J., 2020. Characterization of an intraplate seismogenic zone using geophysical and borehole data: the Vila Franca de Xira Fault, Portugal. Seismol. Res. Lett. 91 (4), 2287–2297. https://doi.org/10.1785/0220190317.
Chávez-Pérez, S., Louie, J.N., Pullammanappallil, Sathish K., 1998. Seismic depth imaging of normal faulting in the southern Death Valley basin. Geophysics 63, 223–230.
Crane, J.M., 2013. Effects of Stress and Water Saturation on Seismic Velocity and Attenuation in Near Surface Sediments, 3714. Louisiana State University Doctoral Dissertations. https://digitalcommons.lsu.edu/gradschool_dissertations/3714.
Custódio, S., Dias, N.a., Carrilho, F., Góngora, E., Rio, I., Marreiros, C., Morais, I., Alves, P., Matias, L., 2015. Earthquakes in western Iberia: improving the understanding of lithospheric deformation in a slowly deforming region. Geophys. J. Int. 203, 127–145.
D'Amato, D., Pace, B., Cabral, J., Figueiredo, P.M., 2009. The Vale de Santarém Neogene trough in the seismotectonics framework of the lower Tagus Valley (Portugal). In: Trabajos de Geología, 29. Universidad de Oviedo, pp. 200–205.
de Vicente, G., Cunha, P.P., Muñoz-Martín, A., Cloetingh, S.A.P.L., Olaiz, A., Vegas, R., 2018. The Spanish-Portuguese Central System: An example of intense intraplate deformation and strain partitioning. Tectonics 37, 4444–4469. https://doi.org/10.1029/2018TC005204.
Dix, C.H., 1955. Seismic velocities from surface measurements. Geophysics 20, 68–86.
Elliot, T., Ladio, K.O., 1981. Syn-sedimentary gravity slides (growth faults) in coal measures of South Wales. Nature 291, 220–222.
Figueiredo, P.M., Cabral, J., Rockwell, T., 2011. Plio-Pleistocene Tectonic Activity in the Southwest of Portugal, 2nd INQUA-IGCP-567 International Workshop on Active Tectonics, Earthquake Geology, Archaeology and Engineering, Corinth, Greece, pp. 1–4.
Floyd, J.S., Mutter, J.C., Goodlife, A.M., Taylor, B., 2001. Evidence of fault weakness and fluid flow within an active low-angle normal fault. Nature 411, 779–783.

Gazdag, J., Squazzero, P., 1984. Migration of seismic data by phase shift plus interpolation. Geophysics 49, 124–131.

Ghose, R., Goudswaard, J., 2004. Integrating S-wave seismic reflection data and cone-penetration-test data using a multiangle multiscale approach. Geophysics 69 (2), 440–459.

Ghose, R., Carvalho, J., Loureiro, A., 2013. Signature of fault zone deformation in near-surface soil visible in shear wave seismic reflections. Geophys. Res. Lett. 40, 1074–1078.

Gold, R.D., Stephenson, W.J., Odum, J.K., Briggs, R.W., Crone, A.J., Angster, S.J., 2013. Concealed Quaternary strike-slip fault resolved with airborne lidar and seismic reflection: the Grizzly Valley fault system, northern Walker Lane, California. J. Geophys. Res. Solid Earth 118, 3753–3766. https://doi.org/10.1002/jgrb.50238.

Harris, J.B., 2009. Hammer-impact SH-wave seismic reflection methods in neotectonic investigations: General observations and case histories from the Mississippi embayment, U.S.A. J. Earth Sci. 20 (3), 513–524.

Harris, J.B., 2010. Application of shallow shear-wave seismic reflection methods in earthquake hazard studies. Lead. Edge 29 (8), 960–963.

Hough, S.E., Ben-Zion, Y., Leary, P., 1994. Fault-zone waves observed at the southern Joshua tree earthquake rupture zone. Bull. Seismol. Soc. Am. 84 (3), 761–767.

Hunter, J.A., Crow, H.L., Stephenson, W.J., et al., 2022. Seismic site characterization with shear wave (SH) reflection and refraction methods. J. Seismol. 26, 631–652. https://doi.org/10.1007/s10950-021-10042-z.

Inazaki, T., 2004. High-Resolution seismic reflection surveying at paved areas using and S-wave type land streamer. Explor. Geophys. 35 (1), 1–6.

Jeng, Y., Tsai, J., Chen, S., 1999. An improved method of determining near-surface. Q. Geophysics. 64, 1608–1617. https://doi.org/10.1190/1.1444665.

Jongmans, D., 1990. In-situ attenuation measurements in soils. Eng. Geol. 29, 99–118.

Kaiser, A.E., Horstmeyer, H., Green, A.G., Campbell, F.M., Langridge, R.M., McClymon, A.F., 2011. Detailed images of the shallow Alpine Fault Zone, New Zealand, determined from narrow-azimuth 3D seismic reflection data. Geophysics 76 (1), 1JF-Z19.

Kawahara, J., Yamashita, T., 1992. Scattering of Elastic Waves by a Fracture Zone Containing Randomly distributed Cracks. PAGEOPH 139 (1), 121–144.

Kudo, K., Shima, E., 1970. Attenuation of shear waves in soil. Bull. Earthq. Res. Inst. 48, 145–158.

LNEG, 2010. Geological Map of Portugal scale 1: 1 000 000, Laboratório Nacional de Energia e Geologia.

Mamada, Y., Kuwahara, Y., Ito, H., Takenaka, H., 2002. 3-D finite-difference simulation of seismic fault zone waves—Application to the fault zone structure of the Mozumi-Sukenobu fault, Central Japan. Earth Planets Space 54, 1055–1058.

Mooney, W.D., Ginzburg, A., 1986. Seismic measurements of the internal properties of fault zones. Pageoph 124 (1/2), 141–157.

Neuwerth, R., Suter, F., Guzman, C.A., Gorin, G.E., 2006. Soft-sediment deformation in a tectonically active area: the Plio-Pleistocene Zarzal Formation in the Cauca Valley (Western Colombia). Sediment. Geol. 186 (1–2), 67–88.

Neves, M.C., Fernandes, R.M., Adam, C., 2014. Refined models of gravitational potential energy compared with stress and strain rate patterns in Iberia. J. Geodyn. 81, 91–104. https://doi.org/10.1016/j.jog.2014.07.010.

Nielsen, L., Thybo, H., Klinkby, L., Abramovitz, T., Balling, N., 1998. Fault detection from back-scattered energy in MONA LISA wide-angle seismic sections from the south-eastern Nort Sea. First Break 14 (4), 119–126.

Nielsen, L., Thybo, H., Jørgensen, M.I., 2005. Integrated seismic interpretation of the Carlsberg Fault zone, Copenhagen, Denmark. Geophys. J. Int. 162, 461–478. https://doi.org/10.1111/j.1365-246X.2005.02664.x.

Onyebueke, E.O., Manzi, M.S.D., Durrheim, R.J., 2018. High-resolution shallow reflection seismic integrated with other geophysical methods for hydrogeological prospecting in the Nylsvley Nature Reserve, South Africa. J. Geophys. Eng. 15 (6), 2658–2673. https://doi.org/10.1088/1742-2140/aadbe3.

Ramos, C., Reis, E., Pereira, A.R., Azevêdo, T.M., Nunes, E., Freitas, M.C., Andrade, C., 2002. Late Holocene evolution of the lower Tagus alluvial plain and heavy metals content: Preliminary results. In: Garcia-Ruiz, J.M., Jones, J.A.A., Armaez, J. (Eds.), Environmental Change and Water Sustainability. Study Group on Water Sustainability of the International Geographical Unit, Zaragoza, pp. 167–182.

Ribeiro, A., Cabral, J., Baptista, R., Matias, L., 1996. Stress pattern in Portugal mainland and the adjacent Atlantic region, West Iberia. Tectonics 15, 641–659.

Rockwell, T., Fonseca, J., Madden, C., Dawson, T., Owen, L.A., Vilanova, S., Figueiredo, P., 2009. Paleoseismology of the Vilariça segment of the Manteigas-Bragança fault in northeastern Portugal. In: Reicherter, K., Michetti, A.M., Silva, P.G. (Eds.), Palaeoseis-mology: Historical and Prehistorical Records of Earthquake Ground Effects for Seismic Hazard Assessment. Geological Society of London Special Publication, pp. 237–258.

Schuster, G..T., Quintus-Bosz, A., 1993. Wavepath eikonal traveltime inversion. Theory. Geophys. 58, 1314–1323. https://doi.org/10.1190/1.1443514.

Shtivelman, V., Frieslander, U., Zilberman, E., Amit, R., 1998. Mapping shallow faults at the Evrona playa site using high-resolution reflection method. Geophysics 15, 1257–1264.

Stirling, M., Rhoades, D., Berryman, K., 2002. Comparison of Earthquake Scaling Relations Derived from Data of the Instrumental and Preinstrumental Era. Bull. Seismol. Soc. Am. 92 (2), 812–830.

Sugiyama, Y., Mizuno, K., Nanayama, F., Sugai, T., Yokota, H., Hosoya, T., Miura, K., Takemura, K., Kitada, N., 2003. Study of blind thrust faults underlying Tokyo and Osaka urban areas using a combination of high-resolution seismic reflection profiling and continuous coring. Ann. Geophys. 46 (5), 1071–1085.

Suter, F., Martínez, J.I., Vélez, M.I., 2011. Holocene soft-sediment deformation of the Santa Fe–Sopetrán Basin, northern Colombian Andes: evidence for pre-Hispanic seismic activity? Sediment. Geol. 235, 188–199. https://doi.org/10.1016/j.sedgeo.2010.09.018.

Thorbecke, J., Draganov, D., 2011. Finite-difference modeling experiments for seismic interferometry. Geophysics 76 (6), H1–H18.

Tün, M., Avdan, U., Kaplan, O., Güney, Y., Çabuk, A., Kaypak, B., Uyar, G., Aldaş, E., Berkan, E., Korhan, S., Gürol, H., 2010. A New Look to the Eskişehir Fault, Extended abstract. In: The 19Th International Geophysical Congress & Exhibition of Turkey, Ankara, Turkey, 23/11/2010, 4 p.

Vanneste, K., Meghraoui, M., Camelbeeck, T., 1999. Late Quaternary earthquake-related soft-sediment deformation along the Belgian portion of the Feldbiss Fault, Lower Rhine Graben system. Tectonophysics 309 (1–4), 57–79.

Vilanova, S.P., Nemser, E., Besana-Ostman, G.M., Bezzeghoud, M., Borges, J.F., da Silveira, A. Brum, Cabral, J., Carvalho, J., Cunha, P.P., Dias, R.P., Madeira, J., Lopes, F.C., Oliveira, C.S., Perea, H., Mayordomo, J. García, Wong, I., Arvidsson, R., Fonseca, J.F., 2014. Incorporating descriptive metadata into seismic source zone models for seismic hazard assessment. Bull. Seismol. Soc. Am. 104, 1212–1229. https://doi.org/10.1785/0120130210.

Wang, S., Li, Z., 2018. S-wave attenuation of the shallow sediments in the North China basin based on borehole seismograms of local earthquakes. Geophys. J. Int. 214 (2), 1391–1400. https://doi.org/10.1093/gji/ggy223.

Watanabe, T., Matsuoka, T., Ashida, Y., 1999. Seismic traveltime tomography using Fresnel volume approach. In: SEG Houston 1999 Meeting, Expanded Abstracts, 10.1190\\1.1820777.

Williams, R.A., Stephenson, W.J., Odum, J.K., Worley, D.M., 2001. Seismic reflection imaging of Tertiary faulting and related post-Eocene deformation 20 km north of Memphis, Tennessee. Eng. Geol. 62 (1–3), 79–90.

Wilson, R.C.L., Hiscott, R.N., Willis, M.G., Gradstein, F.M., 1989. In: Tankard, A.J., Balkwill, H. (Eds.), Extensional Tectonics and Stratigraphy of the North Atlantic Margins, 46. American Association Petroleum Geologists Memoir, pp. 341–361.

Yang, H., Zhu, L., Cochran, E.S., 2011. Seismic structures of the Calico fault zone from local earthquake travel time modeling. Geophys. J. Int. 186, 760–770. https://doi.org/10.1111/j.1365-246X.2011.05055.x.

Zbyszewski, G., Torre de Assunção, C., 1965. Notícia Explicativa da Folha 30-D Alenquer da Carta Geológica de Portugal na escala 1/50.000. Serviços Geológicos de Portugal, Lisboa, p. 104.

Zbyszewski, G., Veiga Ferreira, O., 1967. Folha 31-C Coruche da Carta Geológica de Portugal na escala 1/50.000. Serviços Geológicos de Portugal, Lisboa.

Zbyszewski, G., Veiga Ferreira, O., 1968. Notícia Explicativa da Folha 31-C Coruche da Carta Geológica de Portugal na escala 1/50.000. Serviços Geológicos de Portugal, Lisboa, p. 43.